ADVANCED FUNCTIONAL MATERIALS
www.afm-journal.de

Highly Intensified Surface Enhanced Raman Scattering by Using Monolayer Graphene as the Nanospacer of Metal Film–Metal Nanoparticle Coupling System

Xuanhua Li, Wallace C. H. Choy, Xingang Ren, Di Zhang, and Haifei Lu*

It is widely accepted that surface enhanced Raman scattering (SERS) enhancement results from a combination of electromagnetic mechanisms (EM) and chemical mechanisms (CM). Recently, the nanoparticle-film gap (NFG) system was studied due to its strong local enhancement field. However, there are still some technical limitations in establishing effective and simple ways for reliable and precise control of sub-nanospacer. In addition, works on designing the nanospacer in NFG system for efficient interaction with target molecules for further improving SERS signals are rather limited. Here, a novel NFG system is proposed by introducing ultrathin monolayer graphene as well-defined sub-nanospacer between Ag NPs and Ag film (named G(graphene)-NFG system). The new G–NFG system offers tremendous near-field enhancement with one of the highest enhancement ratio of 1700 reported to date. These results show that the single-layer graphene as a sub-nanospacer renders the proposed G–NFG system with particularly strong EM enhancement (due to multiple couplings including the NP–NP couplings and NP-film couplings) and additional CM enhancement in detecting some π-conjugated molecules to function as a powerful tool in analytical science and the related fields.

1. Introduction

An electromagnetic "hot spot" is a point with a strongly enhanced local field which occurs near sharp asperities and also forms at the small gaps (nanometer or smaller) between metal nanostructures such as nanoparticles (NPs), NP-film system, and.[1–12] In nanoparticle-film-gap (NFG) system, metal NPs (supported localized surface plasmons LSPs) are separated from a bulk metal film (supported surface plasmon polaritons SPPs) by a spacer.[1,2,13–15] One of the interesting features of NFG configuration is that it is widely compatible (at least for most of its construction), which can be popularly adopted in most of typically analytical sciences and the related fields, such as surface-enhanced Raman scattering (SERS), surface-enhanced fluorescence spectra, and other plasmonic sensing with requirements of large area and great spot-to-spot uniformity.[1,13–18] Generally, the aforementioned local field enhancement of hot spots are critically sensitive to the nanoscale spacer (<≈5 nm) between the NP and the film.[1,2,13,14,16,19] Although there are some reports in forming NFG system using dielectric spacer through surface functionalization of the metal film with self-assembled molecular layers,[1,16] the structural integraty of nanosapcer need been further considered. Stable oxide like SiO_2 and Al_2O_3 (≈2 nm or above) produced using conventional physical techniques have also been reported.[14,19] However, there are still some technical limitations in achieving reliable and precise control of sub-nanospacing in the experimental study on coupled plasmonic system. Consequently, a key issue is to find an effective and simple way of realizing a sub-nanospacer with highly structural integrity for further development of NFG system.

It has been widely accepted that SERS enhancement results from a combination of electromagnetic mechanism (EM) and chemical mechanism (CM).[15,20] EM originates from the orders-of-magnitude increase in the local electromagnetic field due to plasmonic resonance,[21] while CM is caused by charge transfer between the target molecules and SERS substrates.[22] The SERS enhancement of EM can reach up to 10^{14} while that of CM is ≈10–100.[22,23] Regarding the NFG system, works about exploring CM enhancement from the nanospacer are rather limited while a lot of works about SERS enhancement of EM have been popularly studied recently.[1,2,13–15] Especially, efficient interaction (e.g., absorbing, concentrating or charge transfer) with the target molecules (e.g., rhodamine 6G (R6G)) is previously inaccessible by using traditional NFG system (with SiO_2 as a nanospacer) due to weak affinity between the NFG system and target molecules. Thus, some advanced designs are highly desirable to further improve the SERS signals from both EM and CM enhancement.

Graphene has attracted intense interest since its experimental discovery.[24–36] The 2-dimensional nature of graphene, its special structure with single planar sheet of sp^2-bonded carbon atoms, and the convenient combination of graphene with plasmonic nanostructures makes it a favorable test bed for investigating the mechanisms of optical response.[37–41] In addition, the ability of graphene to adsorb and concentrate target molecules makes it an attractive candidate for

X. Li, Dr. W. C. H. Choy, X. Ren, D. Zhang, Dr. H. Lu
Department of Electrical and Electronic Engineering
The University of Hong Kong
Pokfulam Road, Hong Kong, China
E-mail: chchoy@eee.hku.hk

DOI: 10.1002/adfm.201303384

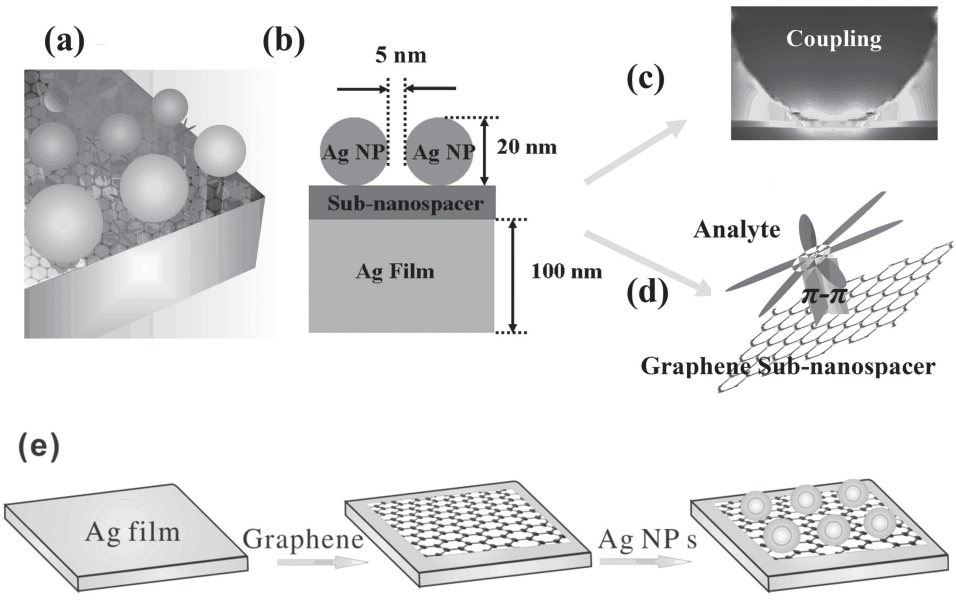

Figure 1. a) 3-dimensional and b) cross-sectional schematic of the G–NFG system, the interesting features the G–NFG system possesses including c) strong near-field due to NPs-film coupling and d) chemical mechanism (CM) enhancement from the monolayer graphene sub-nanospacer through interacting with target analytes owing to strong π–π interaction; and e) schematic of the fabrication process of the graphene separated G–NFG system.

plasmonic sensing applications where molecule-graphene interaction controls the detection enhancement such as SERS enhancement.[24,39,40,42] Nonetheless, the highest graphene enhancement ratio (by dividing the SERS band intensity with the normal Raman band intensity of the graphene) reported to date is less than 1000 at the "hot spot" of plasmonic resonance in the combination system of graphene with plasmonic nanostructures.[10,38,43–45]

In this work, we propose and fabricate a novel NFG system through strategically adopting Ag NPs spaced sub-nanospacer from a Ag film particularly through using monolayer graphene (G–NFG system as shown in **Figure 1**a,b). We experimentally and theoretically demonstrate a significant near-field enhancement. The very strong near-field produced in the proposed graphene sub-nanospacer is due to multiple couplings including the Ag NPs–Ag film coupling and Ag NPs–Ag NPs coupling (see Figure 1c). In addition, we also demonstrate the benefit of as-proposed G–NFG system for further improving the SERS signals through taking advantage of CM enhancement from the graphene nanospacer (see Figure 1d). Consequently, our results contribute to the understanding and applications of new G–NFG system, which simultaneously achieves particularly strong EM enhancement and additional CM enhancement, to become a powerful tool in analytical science and the related fields.

2. Results and Discussion

2.1. G–NFG Geometry

The G–NFG geometry (see Figure 1a,b) is a three-layer structure consisting of the Ag NPs with 20 nm diameter residing on a ultrathin graphene spacer layer covering a Ag film (≈100 nm of Ag deposited on a silicon substrate). The distance of adjacent Ag NPs is about 5 nm. The detailed fabrication process is shown in Figure 1e and Experimental Section. A 100 nm smooth Ag film is firstly evaporated with very slowly evaporating rate (0.1 A s^{-1}) onto Si substrate, followed by transferring a single layer graphene grown on a copper foil via chemical vapor deposition (CVD) onto the Ag film. Subsequently, Ag NPs are evaporated onto the graphene with evaporating rate of 0.7 Å s^{-1} to form the proposed G–NFG system with monolayer graphene sub-nanospacer (i.e., G–NFG system).

Scanning electron microscopy (SEM) and transmission electron microscopy (TEM) are used to observe the surface morphology of different nanostructures involved in the as-proposed G–NFG system, including structures of Ag film (**Figure 2**a), planar Ag film covered by graphene (Figure 2b), planar Ag film on which several nanometer Ag NPs are deposited (Figure 2c), and the G–NFG system (Figures 2d–f). As compared to the geometry of bare Ag film shown in Figure 2a, after graphene is successfully transferred onto the Ag film, there is no obvious change on the morphology and the monolayer graphene has very high transmittance (>90% in the visible wavelength, see Figure S1 in the Supporting Information) as shown in Figure 2b. From Figure 2d,e, we find that the Ag NPs formed on Ag/graphene structure can be clearly observed. By counting about 250 Ag NPs from TEM images, we statistically obtain the size distribution of Ag NPs as shown in Figure 2g and find that the size of the Ag NPs is about 20 nm. Regarding the space separation between Ag NPs, it is only about 5 nm gap obtained from the high-magnification TEM image and the corresponding distance-distribution histogram of the space separation shown in Figures 2f,h, respectively. The very dense distribution of Ag NPs is very beneficial to their coupling for further enhancing the near-field intensity. In our G–NFG system, the graphene sub-nanospacer on Ag film remarkably avoids subsequent migration of the evaporated Ag NPs on the Ag film. It is

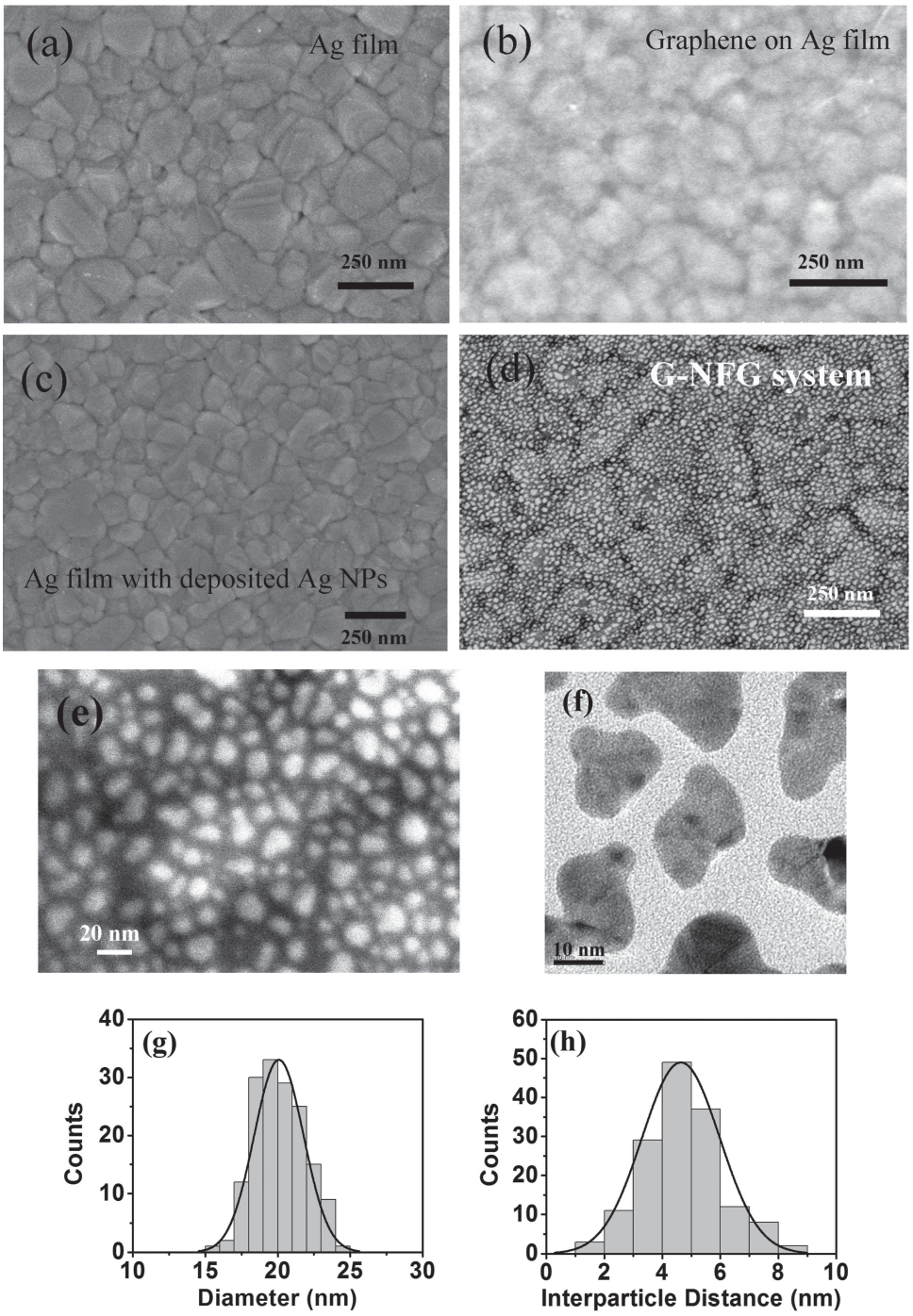

Figure 2. SEM images of various structures used in G–NFG system: a) Ag film, b) monolayer graphene coated Ag film, c) Ag film with an on-top evaporated Ag NPs, and d) G–NFG system. e) High-magnification SEM image of as-fabricated G–NFG system, and f) high-magnification TEM image of as-fabricated G–NFG system. g) Size-distribution histogram of Ag nanoparticles covered onto the Ag film, and h) distance-distribution histogram of interparticle (Ag–Ag) gap.

very different to the case of directly evaporating Ag NPs on Ag film as shown in Figure 2c. The Ag NPs are hardly observed and distinguished from the Ag film without placing graphene sub-nanospacer as a protective net, which further geometrically confirm that the proposed monolayer graphene is efficient as a spacer of G–NFG system.

In order to further characterize the morphology of G–NFG system, especially topography of graphene sub-nanospacer, atomic force microscopy (AFM) images of different structures used in the G–NFG system are measured as shown in Figure S2 in the Supporting Information. Since monolayer graphene is considerably thin and very flexible, the monolayer graphene

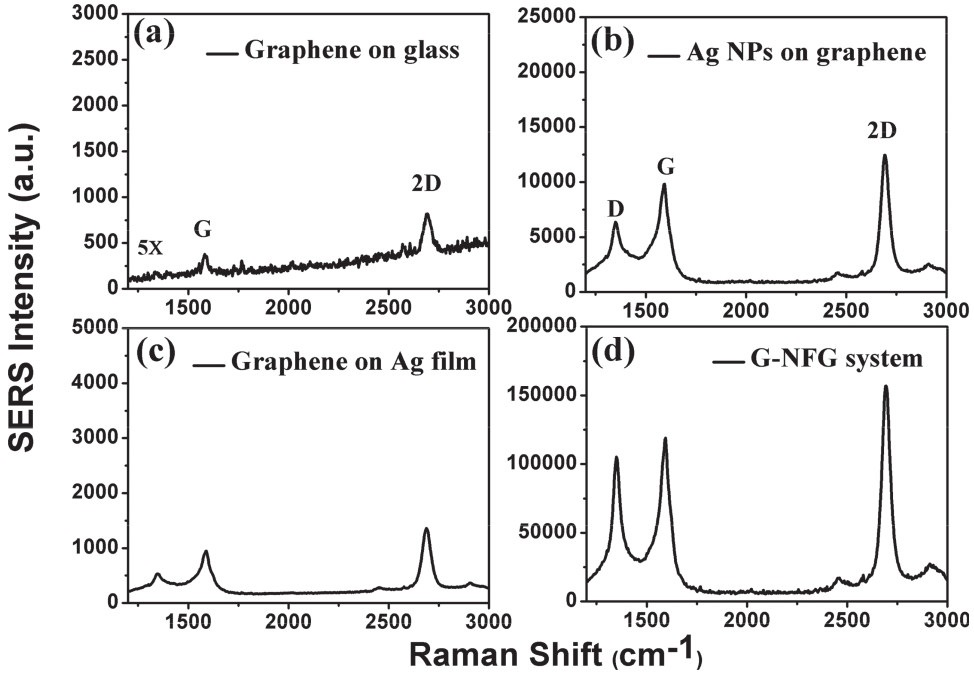

Figure 3. a) Normal Raman spectra of graphene, and SERS spectra of graphene enhanced by different metal nanostructures, including: b) Ag NPs on graphene, c) graphene on Ag film, and d) G–NFG system. The excitation wavelength is 514 nm, the accumulated time is 50 s, and laser power is 5 mW.

can tightly cover the Ag film. Comparing 3-dimensional AFM images of pure Ag film and graphene covered Ag film as shown in Figures S2a,b, Supporting Information, we find there is not clear difference after graphene is introduced onto the Ag film surface. The two structures show similar roughness with root-mean-square roughness 5.842 nm and 6.043 nm for the single Ag film and graphene covered Ag film, respectively, which confirms that the graphene is closely covered onto the underlying Ag film. Figure S2c, Supporting Information, are the AFM image after Ag NPs are evaporated onto the graphene surface, respectively. It can be observed that there are many Ag NPs dispersed on the graphene surface, which are consistent with our SEM results. Based on the clarification using SEM images and AFM images, we can confirm that the graphene sub-nanospacer is tightly formed between the Ag NPs and Ag film to become G–NFG system.

2.2. Remarkably Enhanced SERS in G–NFG System

After constructing the as-proposed monolayer graphene G–NFG system, we study the field enhancement of G–NFG system by detecting the Raman intensity from graphene itself because the SERS intensity directly correlates with the strength of the localized near-field that are enhanced by the surface plasmon coupling between neighboring nanounits.[2,38,45–47] Since graphene has well-known Raman spectrum, it functions as a favorable test bench for investigating the near-field enhancement of the G–NFG system.[11,37,48,49] The strong coupling between the closely distributed Ag NPs and Ag film will induce a dramatic electromagnetic "hot spot" at the graphene sub-nanospacer, and at the same time enhance the Raman signal of graphene nearby. The laser line of 514 nm is chosen to match the plasmon resonances of the as-prepared G–NFG for all the SERS measurement (see absorption spectra of the as-prepared G–NFG system in Figure S3 in the Supporting Information). As shown in **Figure 3**, typical Raman spectra of graphene from samples including monolayer graphene on silica glass (Figure 3a), graphene covered with Ag NPs (Figure 3b), graphene on Ag film (Figure 3c), and G–NFG system with graphene as the sub-nanospacer (Figure 3d) have been investigated. As shown in Figure 3a, the two most intensive features associated with graphene, the G peak around 1580 cm^{-1} and 2D peak around 2685 cm^{-1}, were observed.[38–40,45,46] Particularly, the 2D peak around 2685 cm^{-1} is the signature of monolayer graphene with a single band electronic dispersion.[38,39,45,46] Through the integration of graphene and the double metal structures (Figure 3d), the sample shows additional peak around 1334 cm^{-1} from the D band of carbon, attributed to the lattice deformation caused by the local intensive plasmonic near-field of metal nanostructures.[10,38,43] Furthermore, Raman intensity (both G and 2D peaks) of the graphene with the double metal nanostructures shows significant enhancement as compared to normal Raman spectroscopy from a pristine graphene (graphene on glass), which suggests strong excitation of surface plasmons in metal nanostructures.

We further study the enhancement ratio by dividing the SERS band intensity with the normal Raman band intensity of the graphene. The enhancement ratio for 2D band of monolayer graphene is about 15 and 125 for graphene on Ag film and graphene on Ag NPs, respectively (see Figure 3). Remarkably, when the G–NFG system is introduced, the typical

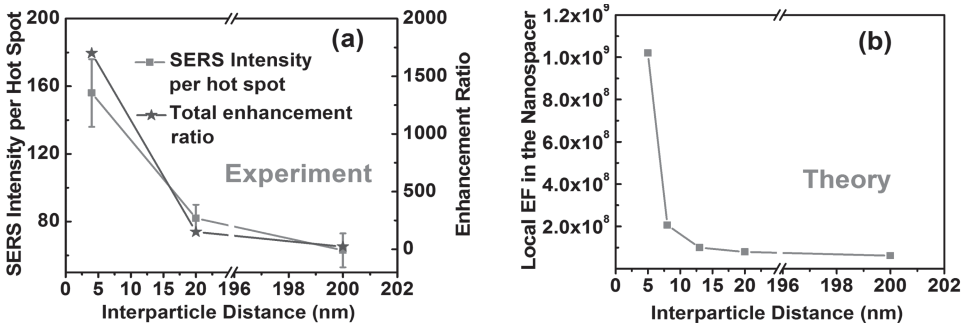

Figure 4. Effect of interparticle distance on the SERS intensity of G–NFG system: a) experimental results and b) theoretical results. For the experimental results, the total enhancement ratio is obtained by dividing the SERS band intensity (graphene combined with plasmonic nanostructures) with the normal Raman band intensity of the graphene (graphene covered on glass). The measured area is the laser spot area. For the theoretical results, the EF is a maximum SERS enhancement factor at the plasmonic spot, which is approximately defined as $|E_{local}/E_0|^4$.

enhancement ratio achieves about 1700, which is nearly 115 times and 14 times larger than that of the graphene on Ag film only and graphene on Ag NPs only, respectively. Interestingly, the enhancement ratio of the graphene for the G–NFG is significantly larger than the simple linear superposition for two individual metal structures with graphene, i.e. graphene on Ag film (SPP from the Ag film) and Ag NPs on graphene (LSP from the Ag NPs). The significant enhancement is promoted due to the multiple plasmonic couplings including the Ag NP-Ag film coupling and Ag NP-Ag NP coupling, which will be further described in our theoretical modeling below. Besides multiple plasmonic coupling, another contributor to the strong Raman enhancement may be from the better superposition of the plasmon resonance of G–NFG SERS substrates with excitation line of 514 nm used in the experiments (see the absorption spectra of different SERS substrate in Figure S3, Supporting Information, and SERS spectra of G–NFG system for three different laser lines (514 nm, 488 nm, and 633 nm) in Figure 3 and Figure S4 in the Supporting Information). When the plasmonic wavelength of SERS substrate is in resonance with the excitation (e.g., the plasmon resonance of G–NFG system matches well with excitation wavelength), the highly intensified Raman enhancement is achieved.[25,44]

It should also be noted that the current graphene Raman enhancement ratio with a value of 1700 is one of the highest enhancement ratio reported to date in the graphene-metal plasmonic combination system. In addition, to our best knowledge, there is no clear surface-enhancement Raman study on a NPs-film coupling system with monolayer graphene sub-nanospacer.

2.3. Effect of Ag Interparticle (NP–NP) Gaps to Raman Enhancement of the G–NFG System

Effect of Ag interparticle (NP–NP) gaps to Raman enhancement of the G–NFG system has also been studied by tuning the distance of interparticle gap. Besides the G–NFG system with closely distributed Ag NPs (5 nm gap, named NP–NP–5nm/G/Film system) discussed above (Figure 2d), we also fabricate another two samples with different interparticle gap, including G–NFG system with sparse Ag NPs (about 200 nm gap) (isolated NP/G/Film) and G–NFG system with relatively dense Ag NPs (about 20 nm gap) (NP–NP-20nm/G/Film) as shown in the SEM images (Figures S5a,b, Supporting Information) and distance-distribution histogram (Figure S5c,d, Supporting Information). From the SEM images of Figure S5a,b, Supporting Information, we find Ag NPs size does not change obviously after the sample is immersed into the acetone. As a result, the change in SERS enhancement is mainly due to the NP–NP gap. To evaluate the Ag NPs coverage, we first count the amount of Ag NPs covered on top of the flat Ag film. There are 1000–1150 NPs, 170–200 NPs, and 12–15 NPs located on the film in one laser spot for the NP–NP–5 nm/G/Film case, NP–NP-20 nm/G/Film case and isolated NP/G/Film case, respectively. The graphene SERS with these samples are shown in Figure 3d, and Figure S5e,f, Supporting Information. For the three structures, the Raman enhancement ratio (2D peak) is 1700, 150, and 23 for NP–NP–5 nm/G/Film case, NP–NP-20 nm/G/Film case and isolated NP/G/Film case, respectively, as compared to normal Raman spectroscopy from pristine graphene (**Figure 4**a). The strong coupling between the Ag NPs and Ag film will induce a dramatic electromagnetic "hot spot" at the graphene sub-nanospacer, and then enhance the Raman signal of the graphene. Thus, the amount of hot spot plays an important role in Raman enhancement. More hot spots will lead to a stronger Raman intensity.

To further clarify the effect of interparticle gap to SERS enhancement of the G–NFG system, we determine the SERS intensity per hot spot between the Ag NPs and Ag film (the details are shown in Figure S6, Supporting Information). Our results show that the SERS intensities per hot spot are about 50–75, 75–88, and 135–165, for isolated NP/G/Film case, NP–NP-20nm/G/Film case, and NP–NP–5nm/G/Film case, respectively, as shown in the Figure 4a, which indicates that the field strength per hot spot is increased along with the decrement of interparticle gap. According to previous report, if the metal NPs is very sparse on the film in the NFG system, the metal NPs become isolated and the interparticle coupling could be neglected.[14] As a result, it is a linear relation between the metal NPs coverage and Raman enhancement.[14] Considering our current case, the metal NPs covered on the film is not isolated (NP–NP–5nm/G/Film case and NP–NP-20 nm/G/Film case) and thus the interparticle coupling should be considered. Interestingly, we note that SERS signal is dramatically

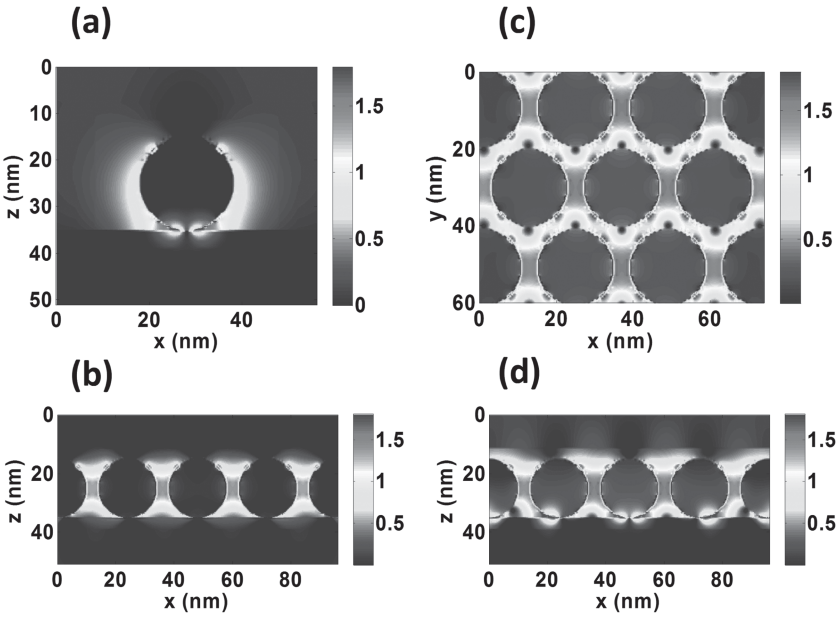

Figure 5. The cross-sectional near field profiles (in log scale) of different nanostructures at excitation wavelength of 514 nm: a) isolated NP/G/Film, b) NP–NP–5 nm/G, and d) NP–NP–5nm/G/Film. c) The top-viewed near field profiles (in log scale) of NP–NP–5 nm/G/Film system at excitation wavelength of 514 nm.

increased along with the decrement of interparticle gap, which indicates that the closer interparticle gap is very beneficial for further enhancing SERS signals (e.g., NP–NP–5 nm/G/Film case).

2.4. Theoretical Modeling about Multiple Plasmonic Couplings in the As-prepared G–NFG System for Strongly Enhanced SERS

To better understand the nature of the strong near-field enhancement in the G–NFG system, we have conducted a theoretical study on the system (Details are described in SI) in which the optical interactions between Ag NPs themselves as well as between Ag NPs and Ag film have been fully considered. In fact, previous studies about the NPs-film system generally focused on the mutual coupling between upper NPs and lower metal film;[13,14,16] and there is little study to consider the interparticle coupling. In our current experimental samples, the interparticles coupling (5 nm gap) is so close that NP–NP and NP-film couplings simultaneously exist which will contribute to the overall enhancement and will be further described below.

In order to systematically study the optical interactions, three structures have been investigated including a isolated Ag NP on a Ag film separated by graphene sub-nanospacer (isolated NP/G/Film, see **Figure 5**a), closely distributed Ag NPs with 5nm gap sitting on graphene (NP–NP/G, see Figures 5b) as well as closely distributed Ag NPs on a Ag film separated by graphene sub-nanospacer (NP–NP–5nm/G/Film, see Figures 5c,d). From the results, we note that graphene exhibits good penetrability so that the electric field can efficiently pass through the monolayer graphene sub-nanospacer, which is consistent with the previous results that the thin graphene layer itself will not induce the clearly electric field attenuation between metal nanostructures.[47,50]

For the case of isolated NP/G/Film, the hot spot appears to be around the region of sub-nanospacer and the EF at the sub-nanospacer is 6.17×10^7 (Figure 5a), where EF is approximately defined as $|E_{local}/E_0|^4$. When many Ag NPs bring together with very small gap of 5 nm sitting on graphene (NP–NP case) as shown in Figures 5b, the enhanced field strength with local EF value of 1.68×10^6 is obtained at the small gap. For the case of NP–NP–5 nm/G/Film case, the multiple plasmonic couplings between the closely distributed Ag NPs as well as between the Ag NPs and the Ag film separated by graphene sub-nanospacer are simutaneously observed (Figures 5c,d). Interestingly, the enhanced field located in the spacer between Ag NPs and Ag film is dramatically boosted and the corresponding EF increases to 1.02×10^9 as shown in Figures 5c,d, which is stronger than that of isolated NP/G/Film case (EF of 6.17×10^7). Theoretical modeling is also conducted to study effect of Ag interparticle (NP–NP) gaps to Raman enhancement of the G–NFG system. As shown in Figure 4b and Figure S7 (Supporting Information), the local field enhancement in the sub-nanospacer strongly increases when the interparticle space decreases. Thus, our theoretical results also reveal a greater field enhancement for the G–NFG system due to multiple plasmonic coupling.

The multiple pasmonic coupling plays a very important role in the G–NFG system. On one hand, the multiple couplings considerably strengthen the near-field on the ultrathin graphene spacer layer and efficiently enhance Raman signals from graphene itself. On the other hand, an additional chemical enhancement from the graphene sub-nanospacer along with the very strong field enhancement at the graphene sub-nanospacer can also offer a unique opportunity for using G–NFG system in highly sensitive analyte characterization (discussed below) (see **Figure 6**a).

2.5. Highly Sensitive Sensors Based on G–NFG System

Regarding the potential applications, we investigate the sensing capability of the as-prepared G–NFG system in detecting a typical organic analyte R6G as an example using SERS technique (see Figure 6). For comparison, we also fabricate two structures including closed distributed Ag NPs with interparticle gap (5 nm) system on silica (SiO_2) glass (NP–NP–5 nm/no G) and closed distributed Ag NPs with interparticle gap (5 nm) system on the graphene film (NP–NP–5 nm/G). To prepare the sample for R6G detection, droplets (of size ≈ 2 mm) of R6G (1×10^{-9} M) solution in ethanol are dropped on the sample, and then samples were dried in air for 2 min to immobilize the molecules on the substrate surface. (see experimental section for detailed Raman measurement). Figure 6b shows the SERS spectra of

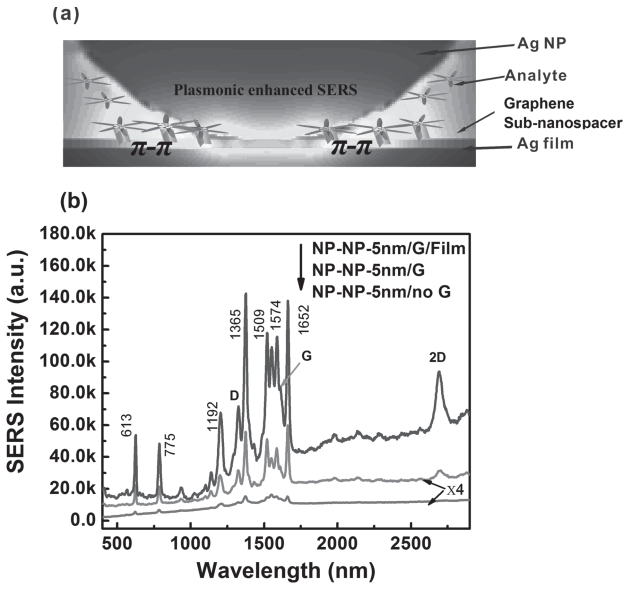

Figure 6. a) Scheme of detection of organic molecule by using as-prepared G–NFG system. SERS performance of G–NFG (NP–NP–5 nm/G/Film) system compared with that of NP–NP–5 nm/no G and NP–NP–5 nm/G structures in detecting R6G with 1×10^{-9} M in ethanol. The excitation wavelength is 514 nm. The accumulated time is 50 s, and laser power is 2 mW.

R6G from three structures including NP–NP–5 nm/no G case, NP–NP–5 nm/G case and NP–NP–5 nm/G/Film case. The positions of the characteristic peaks including 1652, 1574, 1509, 1365, 1192, 775, and 613 cm^{-1} attributed to R6G are generally in agreement with those reported previously.[3,40,45] For the SERS of R6G on the NP–NP–5 nm/G substrate and NP–NP–5 nm/G/Film substrate, the monolayer graphene Raman peaks are also observed. Compared the NP–NP–5 nm/no G case with NP–NP–5nm/G case, we find the Raman intensity of R6G is enhanced (by approximately a factor of 10) by introducing graphene on the bottom of Ag NPs. It has been reported that monolayer graphene facilitates charge transfer between graphene and probe molecules, resulting in a vibration-mode dependent enhancement of 2–17 times.[39] Secondly, aromatic molecules prefer to stack in parallel to the π-bonds of graphene through π-π stacking and lead to enhanced resonant energy transfer.[47] This is further supported by the handful of experimental papers reporting the SERS effect from graphene, which belongs to chemical enhancement mechanism (CM).[24,39,40,42,48–53] In contrast, SERS enhancement from CM is not clearly observed from SiO_2 film when SERS performance is compared from NP–NP–5 nm/SiO_2 case and NP–NP–5 nm/G case.

Furthermore, when the NP–NP–5 nm/G/Film substrate is introduced, the SERS intensity are enormously boosted. The intensity of SERS (i.e., peak in 1652 cm^{-1}) on the NP–NP–5 nm/G/Film substrate are 105–000 units, which means our NP–NP–5 nm/G/Film system can generate 13-fold and 130-fold stronger signal in detecting R6G molecules compared with that of NP–NP–5 nm/G substrate and NP–NP–5 nm/no G substrate, respectively. The highly intensified SERS sensitivity is mainly attributed to the greater field enhancement for the NP–NP–5 nm/G/Film system through multiple plasmonic coupling including NP–NP coupling and NP-film coupling along with the additional CM enhancement from graphene nanospacer (see Figure 6a). We also evaluate the enhancement effect of G–NFG system by comparing with that of traditional NFG system, which has been widely demonstrated as SERS-active substrates. As shown in Figure S8 (Supporting Information), our G–NFG system can generate 6.5 times stronger signal in detecting R6G molecules. Consequently, through the study of a π-conjugated molecule, the monolayer graphene sub-nanospacer in the G–NFG system strengthens the ability to interact with target molecules which makes G–NFG become an attractive system for SERS detection.

The graphene introduced into the NPs-film coupling system serves several distinct purposes. From the construction of view, the graphene is the first time to be used as a ultrathin protective net to achieve a NPs-film coupling system. Its 2-dimensional thickness enables the spacer so close up to sub-nanometer and its 2-dimensional structure make the spacer so integrated, which at the same time overcomes the limitation to fabricate the sub-nanospacer for metal oxide spacer and to improve the integrity of the self-assembly organic molecules spacer in the NPs-film coupling system. From the plasmonic point of view, the graphene is a Raman active membrane that serves as a detection channel of the near-field distribution. From the sensor application, the graphene nanospacer could offer additional CM enhancement to improve the total SERS signal, which can further extend the NFG system application in effectively detecting molecules.

3. Conclusions

We have proposed a novel G–NFG system by introducing ultrathin monolayer graphene as well-defined sub-nanospacer with high structural integrity between Ag NPs and Ag film. Our results show that the G–NFG system offers tremendous near-field enhancement with one of the highest enhancement ratio (1700) reported to date in the graphene-metal plasmonic combination system. Particularly, the strong EM enhancement at the sub-nanospacer and additional CM enhancement from the graphene sub-nanospacer offer a very useful opportunity for the characterization of adsorbed molecules on a wide range of graphene surfaces by efficient enhancement of Raman scattering, which is previously inaccessible by using traditional NFG system (i.e., SiO_2 as a nanospacer in a NFG system). Our experimental and theoretical results show that the enhancement can be explained due to the multiple couplings between Ag NPs as well as between the Ag film and Ag NPs. By detecting R6G as an example, we show that the G–NFG system can be used to realize very sensitive detection of π-conjugated molecule due to both EM enhancement and CM enhancement. Furthermore,we strongly believe that this simple and reliable method would offer stepping stones for enabling quantitative plasmonic sensing at single molecule level. Our results show that the proposed G–NFG system can function as a powerful tool in analytical science and the related fields.

It should be noted that even though the Ag nanostructures show a large distribution and non-uniformity in the as-proposed

G–NFG system (shown in Figure 2), the issue will not affect our results. It is because taking the case of 5 nm interparticle gap in the G–NFG system as an example, the SERS signal obtained from one laser spot is an integrated effect from 1000–1150 Ag NPs (see the relative information in the part: Raman enhancement for per hot spot in the Supporting Information). In addition, in the presented results, we have taken three SERS spectra in different positions of the substrate and then averaged them for each sample, which further make the results reliable (see the Experimental Section). On the other hand, finding a way of realizing highly uniform 2-D NPs in our G–NFG system will be useful and significant in the industrial implementation. Recently, several interesting works have been reported in achieving highly uniform 2-D nanopatterns[54,55] or 2-D close-packed nanoparticle array,[56,57] which contribute to enabling highly-uniform depositions of nanoparticles on NFG systems. The methods will be explored and studied in the future.

When our current work is being reviewed, two work about graphene as a sub-nanogap for tuning plasmon resonance through different perspective have been reported.[58,59]

4. Experimental Section

The G–NFG System Fabrication: a thin layer of chromium (Cr, 5 nm) was firstly evaporated onto the silicon substrate as the adhesion layer. Then 100 nm smooth Ag film was evaporated with very slowly evaporation rate (0.1 Å s^{-1}) onto the Cr covered silicon substrate, followed by transferring a single layer graphene grown on a copper foil (obtained from Graphene Supermarket) by traditional solution method.[31,32,45–47] In order to transfer the graphene film onto the Ag film, polymethyl methacrylate (PMMA) was first spin-coated on the surface of the as-grown graphene on copper, followed by 30 min of thermal treatment for drying the PMMA film. The sample was then placed in iron (III) chloride solution (20mg/ml) to remove the copper foil, followed by rinsing with deionized (DI) water, soaking in DI water, and then being transferred to an Ag film. The sample was then baked on a hot plate at 100 °C for 1 h to eliminate moisture before the PMMA was removed by using acetone. Subsequently, Ag NPs were evaporated onto the graphene with evaporating rate (0.7 Å s^{-1}) to form the proposed G–NFG substrate with monolayer graphene as sub-nanospacer. The distance of interparticle gap is about 5 nm. To fabricate the G–NFG system with different interparticle distance, we can remove partial NPs on top of Ag film by immersing the samples into acetone for different time. The acetone will infiltrate into the interface region between the NPs and graphene easily, which make the NPs strip out. According to our experimental results, we find that the longer time the NPs immerse into the acetone, the more the NPs strip out. In our current experiment, the time are 120 min and 50 min for the G–NFG system with sparse Ag NPs and dense Ag NPs (interparticle distance 20 nm), respectively. The fabrication of standard NFG system was similar to that of the G–NFG system. To create nanospacer layers with controllable thickness with just a few angstroms, self-assembled monolayers (SAMs) of amine-terminated alkanethiols on Ag film were fabricated using chain lengths of $n = 2$ where n equals the number of carbon atoms along the alkane portion of the molecule based on the previous report.[1] The SAMs do not show obvious π-conjugated effect.

Microscopic and Optical Characterization: The morphology of samples was characterized using scanning electron microscopy (SEM; Hitachi S-4800) and atomic force microscopy (AFM, Asylum Research MFP-3D) in tapping mode. The TEM image of Ag nanomaterials was measured using Philips Tecnai G2 20 S-TWIN. The sample for TEM measurement were prepared by firstly transferring the single layer graphene to copper (Cu) grids and subsequently evaporating Ag NPs onto the graphene. The absorption spectra of SERS substrates were extracted from the diffuse reflection (*R*) and transmission spectra (*T*) (1-*T*-*R*) using a goniometer combined with a CCD spectrometer and integrating sphere.[60,61]

SERS for Molecule Detection: Raman spectra were obtained using a horiba HR800 Raman system with a 514 nm laser. For each sample, we took three SERS spectra in different positions of the substrate and then averaged them. To prepare the sample for R6G detection, droplets (of size ≈ 2 mm) of R6G (1×10^{-9} M) solution in ethanol are dropped on the sample, and then samples were dried in air for 2 min to immobilize the molecules on the substrate surface. The accumulated time of Raman measurement was 50 s; and laser power at the sample position was 2 mW for R6G. For detecting the Raman spectrum of monolayer graphene, the laser power at the sample position was 5 mW and the accumulation time used for the study was 50 s.

Theoretical Modeling: Maxwell's equations were solved utilizing the finite-difference time-domain (FDTD) method to better understand the nature of the strong near-field enhancement in the G–NFG system.[62] Details are described in the Supporting information.

Supporting Information

Supporting Information is available from the Wiley Online Library or from the author.

Acknowledgement

This work is supported by University Grant Council of the University of Hong Kong (grants #4002343 and #201111159062), the General Research Fund (grants: HKU711612E), the RGC-NSFC grant (N_HKU709/12) and CRF grant (CUHK1/CRF/12G) from the Research Grants Council of Hong Kong Special Administrative Region, China. The authors thank L. C. W. Dennis and Theresa Mei for part of the SERS measurement.

Received: October 1, 2013
Revised: December 11, 2013
Published online: January 28, 2014

[1] C. Ciraci, R. T. Hill, J. J. Mock, Y. Urzhumov, A. I. Fernandez-Dominguez, S. A. Maier, J. B. Pendry, A. Chilkoti, D. R. Smith, *Science* **2012**, *337*, 1072.
[2] J. F. Li, Y. F. Huang, Y. Ding, Z. L. Yang, S. B. Li, X. S. Zhou, F. R. Fan, W. Zhang, Z. Y. Zhou, Y. W. De, B. Ren, Z. L. Wang, Z. Q. Tian, *Nature* **2010**, *464*, 392.
[3] X. Li, G. Chen, L. Yang, Z. Jin, J. Liu, *Adv. Funct. Mater.* **2010**, *20*, 2815.
[4] K. J. Savage, M. M. Hawkeye, R. Esteban, A. G. Borisov, J. Aizpurua, J. J. Baumberg, *Nature* **2012**, *491*, 574.
[5] H. M. Chen, C. K. Chen, M. L. Tseng, P. C. Wu, C. M. Chang, L. C. Cheng, H. W. Huang, T. S. Chan, D. W. Huang, R. S. Liu, D. P. Tsai, *Small* **2013**, *9*, 2926.
[6] L. Yang, L. Ma, G. Chen, J. Liu, Z.-Q. Tian, *Chem. Eur. J.* **2010**, *16*, 12683.
[7] Y. Zhang, J. Qian, D. Wang, Y. Wang, S. He, *Angew. Chem. Int. Ed.* **2013**, *52*, 1148.
[8] L. Zhang, C. Jiang, Z. Zhang, *Nanoscale* **2013**, *5*, 3773.
[9] R. B. Jiang, H. J. Chen, L. Shao, Q. Li, J. F. Wang, *Adv. Mater.* **2012**, *24*, 200.
[10] J. Lee, S. Shim, B. Kim, H. S. Shin, *Chem. Eur. J.* **2011**, *17*, 2381.
[11] J. Lee, K. S. Novoselov, H. S. Shin, *ACS Nano* **2011**, *5*, 608.
[12] A. L. Stepanov, *Rev. Adv. Mater. Sci.* **2010**, *26*, 1.
[13] Y. Z. Chu, M. G. Banaee, K. B. Crozier, *ACS Nano* **2010**, *4*, 2804.

[14] S. Mubeen, S. P. Zhang, N. Kim, S. Lee, S. Kramer, H. X. Xu, M. Moskovits, *Nano Lett.* **2012**, *12*, 2088.
[15] J. F. Li, S. Y. Ding, Z. L. Yang, M. L. Bai, J. R. Anema, X. Wang, A. Wang, D. Wu, B. Ren, S. Hou, T. Wandlowski, Z. Q. Tian, *J. Am. Chem. Soc.* **2011**, *133*, 15922.
[16] F. Schertz, M. Schmelzeisen, R. Mohammadi, M. Kreiter, H. J. Elmers, G. Schonhense, *Nano Lett.* **2012**, *12*, 1885.
[17] X. Y. Xuan, S. P. Xu, Y. Liu, H. B. Li, W. Q. Xu, J. R. Lombardi, *J. Phys. Chem. Lett.* **2012**, *3*, 2773.
[18] A. Chen, R. L. Miller, A. E. DePrince, A. Joshi-Imre, E. Shevchenko, L. E. Ocola, S. K. Gray, U. Welp, V. K. Vlasko-Vlasov, *Small* **2013**, *9*, 1939.
[19] C. Lumdee, S. Toroghi, P. G. Kik, *ACS Nano* **2012**, *6*, 6301.
[20] A. Campion, P. Kambhampati, *Chem. Soc. Rev.* **1998**, *27*, 241.
[21] H. Xu, J. Aizpurua, M. Kall, P. Apell, *Phys. Rev. E* **2000**, *62*, 4318.
[22] B. N. J. Persson, K. Zhao, Z. Zhang, *Phys. Rev. Lett.* **2006**, *96*, 207401.
[23] A. Otto, I. Mrozek, H. Grabhorn, W. J. Akemann, *Phys: Condens. Matter* **1992**, *4*, 1143.
[24] G. Sarau, B. Lahiri, P. Banzer, P. Gupta, A. Bhattacharya, F. Vollmer, S. Christiansen, *Adv. Optical Mater.* **2013**, *1*, 151.
[25] P. Wang, O. Liang, W. Zhang, T. Schroeder, H. Xie, *Adv. Mater.* **2013**, *25*, 4918.
[26] J. M. Yuk, K. Kim, B. Aleman, W. Regan, J. H. Ryu, J. Park, P. Ercius, H. M. Lee, A. P. Alivisatos, M. F. Crommie, J. Y. Lee, A. Zettl, *Nano Lett.* **2011**, *11*, 3290.
[27] V. Georgakilas, M. Otyepka, A. B. Bourlinos, V. Chandra, N. Kim, K. C. Kemp, P. Hobza, R. Zboril, K. S. Kim, *Chem. Rev.* **2012**, *112*, 6156.
[28] F. N. Xia, T. Mueller, Y. M. Lin, A. Valdes-Garcia, P. Avouris, *Nat. Nano.* **2009**, *4*, 839.
[29] N. M. Gabor, J. C. W. Song, Q. Ma, N. L. Nair, T. Taychatanapat, K. Watanabe, T. Taniguchi, L. S. Levitov, P. Jarillo-Herrero, *Science* **2011**, *334*, 648.
[30] H. Chang, H. Wu, *Adv. Funct. Mater.* **2012**, *23*, 1984.
[31] J. C. Reed, H. Zhu, A. Y. Zhu, C. Li, E. Cubukcu, *Nano Lett.* **2012**, *12*, 4090.
[32] D. Zhang, F. X. Xie, P. Lin, W. C. H. Choy, *ACS Nano* **2013**, *7*, 1740.
[33] X. Li, D. Xie, H. Park, T. H. Zeng, K. Wang, J. Wei, M. Zhong, D. Wu, J. Kong, H. Zhu, *Adv. Energy Mater.* **2013**, *3*, 1029.
[34] E. Shi, H. Li, L. Yang, L. Zhang, Z. Li, P. Li, Y. Shang, S. Wu, X. Li, J. Wei, K. Wang, H. Zhu, D. Wu, Y. Fang, A. Cao, *Nano Lett.* **2013**, *13*, 1776.
[35] S. H. Mousavi, I. Kholmanov, K. B. Alici, D. Purtseladze, N. Arju, K. Tatar, D. Y. Fozdar, J. W. Suk, Y. F. Hao, A. B. Khanikaev, R. S. Ruoff, G. Shvets, *Nano Lett.* **2013**, *13*, 1111.
[36] X. Li, R. J. Zhang, W. J. Yu, K. L. Wang, J. Q. Wei, D. H. Wu, A. Y. Cao, Z. H. Li, Y. Cheng, Q. S. Zheng, R. S. Ruoff, H. W. Zhu, *Sci. Rep.* **2012**, *2*, 870.
[37] H. Tian, H. Y. Chen, B. Gao, S. M. Yu, J. L. Liang, Y. Yang, D. Xie, J. F. Kang, T. L. Ren, Y. G. Zhang, H. S. P. Wong, *Nano Lett.* **2013**, *13*, 651.
[38] G. W. Xu, J. W. Liu, Q. Wang, R. Q. Hui, Z. J. Chen, V. A. Maroni, J. Wu, *Adv. Mater.* **2012**, *24*, 71.
[39] X. Ling, L. M. Xie, Y. Fang, H. Xu, H. L. Zhang, J. Kong, M. S. Dresselhaus, J. Zhang, Z. F. Liu, *Nano Lett.* **2010**, *10*, 553.
[40] E. S. Thrall, A. C. Crowther, Z. H. Yu, L. E. Brus, *Nano Lett.* **2012**, *12*, 1571.
[41] V. G. Kravets, F. Schedin, R. Jalil, L. Britnell, K. S. Novoselov, A. N. Grigorenko, *J. Phys. Chem. C* **2012**, *116*, 3882.
[42] M. A. Creighton, J. R. Rangel-Mendez, J. Huang, A. B. Kane, R. H. Hurt, *Small* **2013**, *9*, 1921.
[43] C. E. Cheng, C. Y. Lin, H. Y. Chang, C. H. Huang, H. Y. Lin, C. H. Chen, C. C. Hsu, C. S. Chang, F. S. S. Chien, *Opt. Express* **2013**, *21*, 6547.
[44] Q. Z. Hao, B. Wang, J. A. Bossard, B. Kiraly, Y. Zeng, I. K. Chiang, L. Jensen, D. H. Werner, T. J. Huang, *J. Phys. Chem. C* **2012**, *116*, 7249.
[45] P. Wang, W. Zhang, O. Liang, M. Pantoja, J. Katzer, T. Schroeder, Y. H. Xie, *ACS Nano* **2012**, *6*, 6244.
[46] S. Heeg, R. Fernandez-Garcia, A. Oikonomou, F. Schedin, R. Narula, S. A. Maier, A. Vijayaraghavan, S. Reich, *Nano Lett.* **2013**, *13*, 301.
[47] J. J. Mock, R. T. Hill, Y. Tsai, A. Chilkoti, D. R. Smith, *Nano Lett.* **2012**, *12*, 1757.
[48] W. G. Xu, J. Q. Xiao, Y. F. Chen, Y. B. Chen, X. Ling, J. Zhang, *Adv. Mater.* **2013**, *25*, 928.
[49] Q. Z. Hao, Y. Zeng, B. K. Juluri, X. D. Wang, B. Kiraly, I. K. Chiang, L. Jensen, D. H. Werner, V. H. Crespi, T. J. Huang, *ACS Nano* **2011**, *5*, 5472.
[50] R. Rao, R. Podila, R. Tsuchikawa, J. Katoch, D. Tishler, A. M. Rao, M. Ishigami, *ACS Nano* **2011**, *5*, 1594.
[51] W. G. Xu, X. Ling, J. Q. Xiao, M. S. Dresselhaus, J. Kong, H. X. Xu, Z. F. Liu, J. Zhang, *Proc. Natl. Acad. Sci. U. S. A.* **2012**, *109*, 9281.
[52] S. Murphy, L. Huang, P. V. Kamat, *J. Phys. Chem. C* **2013**, *117*, 4740.
[53] X. Ling, L. Moura, M. A. Pimenta, J. Zhang, *J. Phys. Chem. C* **2012**, *116*, 25112.
[54] T. F. Kuech, L. J. Mawst, *J. Phys. D: Appl. Phys.* **2010**, *43*, 183001.
[55] G. Liu, H. Zhao, J. Zhang, J. H. Park, L. J. Mawst, N. Tansu, *Nanoscale Res. Lett.* **2011**, *6*, 342.
[56] P. Kumnorkaew, Y. Ee, N. Tansu, J. F. Gilchrist, *Langmuir*, **2008**, *24*, 12150.
[57] W. H. Koo, W. Youn, P. Zhu, X. Li, N. Tansu, F. So, *Adv. Funct. Mater.* **2012**, *22*, 3454.
[58] L. Sha, X. Wang, H. Xu, J. Wang, J. Xu, L. Peng, H. Lin, *Adv. Optical Mater.* **2013**, DOI: 10.1002/adom.201300313.
[59] J. Cheng, W. Wang, H. Mosallaei, E. Kaxiras, *Nano Lett.* **2014**, *14*, 50.
[60] X. H. Li, W. C. H. Choy, L. J. Huo, F. Xie, W. E. I. Sha, B. Ding, Y. Li, J. Hou, J. You, Y. Yang, *Adv. Mater.* **2012**, *24*, 3046.
[61] X. H. Li, W. C. H. Choy, X. G. Ren, J. Xin, P. Lin, C. H. Leaug, *Appl. Phys. Lett.* **2013**, *102*, 153304.
[62] X. G. Ren, Z. X. Huang, X. L. Wu, S. L. Lu, H. Wang, L. Wu, S. Li, *Comput. Phys. Commun.* **2012**, *183*, 1192.